

Rain Attenuation Characteristics due to Typhoon Wind Velocities in Satellite Communications

Yasuyuki MAEKAWA^{†a)} and Yoshiaki SHIBAGAKI[†], Members

SUMMARY Rain attenuation characteristics due to typhoon passage are discussed using the Ku-band BS satellite signal observations conducted by Osaka Electro-Communication University in Neyagawa from 1988 to 2019. The degree of hourly rain attenuation due to rainfall rate is largely enhanced as typhoon passes the east side of the station, while it becomes smaller in the case of west side passage. Compared to hourly ground wind velocities of nearby AMeDAS, the equivalent path lengths of rain attenuation become larger as the wind directions approach the same angle to the satellite, while they become smaller as the wind directions approach the opposite angle to the satellite. The increase and decrease of the equivalent path lengths are confirmed in other Ku-band and Ka-band satellite paths with different azimuth angles, such as CS, SKP, and SBC. Modified equivalent path lengths calculated by a simple propagation path model including horizontal wind speeds along the same direction to the satellite agree well with the equivalent path lengths observed by each satellite. The equivalent path lengths are, for the first time, proved to be largely affected by the direction of typhoon passage and the horizontal wind velocities.

key words: satellite communications, rain attenuation, equivalent path length, typhoon, wind velocity

1. Introduction

It is well known that rain attenuation become significant in satellite communications using frequencies of higher than 10 GHz [1]–[3]. Rain attenuation statistics are usually predicted by long-term rainfall rate statistics observed on the ground. Typical statistical values used in the predictions, such as the ITU-R recommendations, are long-term average of the rainfall rate with the time percentage of 0.01% and average 0°C isotherm height [4]. The equivalent path lengths are, however, found to show considerable variations depending on the ground temperature and rain types, by our previous studies using Ku-band (BS, 11.84 GHz) and Ka-band (CS, 19.45 GHz) satellite signal observations conducted at Osaka Electro-Communication University in Neyagawa, Japan [5].

In this study, the degree of hourly rain attenuation due to rainfall rate is investigated in relation to typhoon passage which frequently occurs in summer and autumn. The rain attenuation characteristics due to typhoon wind velocities are studied in light of variations of equivalent path length obtained from each rainfall event for the past 32 years from 1988 to 2019. Ku-band radio wave attenuation is measured

Table 1 Satellite signals used in the measurements.

	Frequency	Azimuth	Elevation	Period
BS	11.84 GHz	220.1 deg	41.3 deg	1988-2019
CS	19.45 GHz	186.4 deg	49.5 deg	1988-2005
SKP	12.6 GHz	193.2 deg	48.8 deg	2004-2019
SBC	12.7 GHz	165.5 deg	48.6 deg	2004-2019

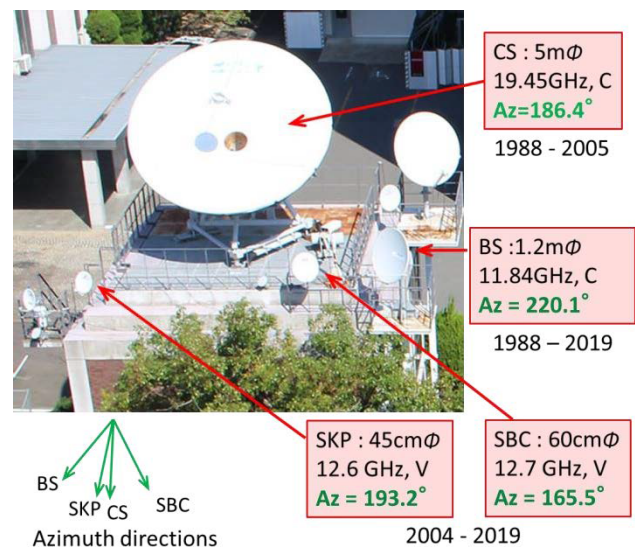


Fig. 1 Observation systems and locations of antennas used in the measurements at OECU in Neyagawa.

by the BS signal (BS, 11.84 GHz, circular polarization) using an IF level meter. At the same time, Ka-band attenuation is measured by CS-2, CS-3, and N-STAR beacon signals (CS, 19.45 GHz, circular) using a beacon receiver up to 2005. Also, Ku-band attenuation in different azimuth angles is measured by JCSAT-3 (SKP, 12.6 GHz, vertical) and SUPERBIRD-C (SBC, 12.7 GHz, vertical) using IF-level meters since 2004. Table 1 summarizes the specification and observation period of these satellite signals used in the measurements at Osaka Electro-Communication University (OECU). The observation systems and the locations of antennas are also shown in Fig. 1. Azimuth angles are here indicated clockwise from northward (0 deg).

2. Examples of Rain Attenuation

First, examples of rain attenuation characteristics are presented using the rainfall events obtained on August 7 and September 17–18, 2017 in Neyagawa observation station.

Manuscript received June 15, 2021.

Manuscript revised October 14, 2021.

Manuscript publicized December 3, 2021.

[†]The authors are with Osaka Electro-Communication University, Neyagawa-shi, 572-8530 Japan.

a) E-mail: maekawa@osakac.ac.jp

DOI: 10.1587/transcom.20211SP0008

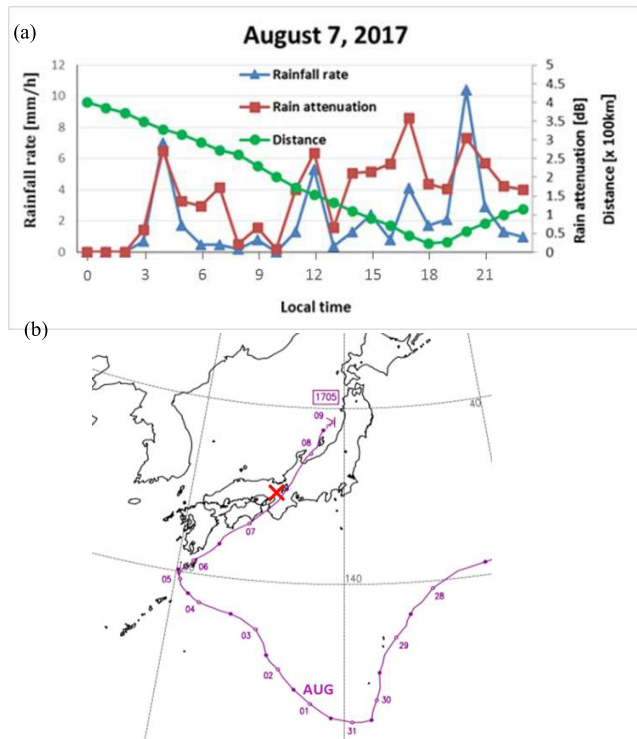


Fig. 2 (a) Rainfall rate and Ku-band rain attenuation together with typhoon distance [6] obtained on August 7, 2017, and (b) the typhoon route published by Japan Meteorological Agency [7]. The observation point (OECU) is marked by a red cross (X).

Figure 2(a) shows the rainfall rate and rain attenuation observed on August 7, 2017, together with the distance of the typhoon center from the observation station. These observed values are averaged over one hour in accordance with the record of typhoon distance, obtained from the location of the typhoon center in the Website of Digital Typhoon [6]. On the other hand, Fig. 2(b) shows the typhoon route published by Japan Meteorological Agency [7]. The circles attached to the curve with the date mean the location of the typhoon center at 0 LT on each day. From Fig. 2(b), the typhoon is shown to pass the east side of the observation station in Neyagawa, Osaka. This observation point is marked by a red cross (X).

It is found in Fig. 2(a) that as the typhoon approaches the station down to nearly 20 km during 17–19 LT, the rain attenuation is increased up to 4 dB while the rainfall rate stays about 4 mm/h. So, the degree of rain attenuation due to rainfall rate is largely enhanced in this situation. Around this time of 17 LT, a strong hourly northeasterly wind of 7.5 m/s was detected by the ground wind data of Hirakata AMeDAS (Automated Meteorological Data Acquisition System) of Japan Meteorological Agency [8], which is located 6.8 km northeast from Neyagawa station.

Figure 3(a) similarly depicts rainfall rate, rain attenuation, and typhoon distance [6] obtained on September 17–18, 2017. Also, Fig. 3(b) indicates the typhoon route [7]. In this case, the typhoon is shown to pass the west side of the observation station (X) in Neyagawa, Osaka. It should be

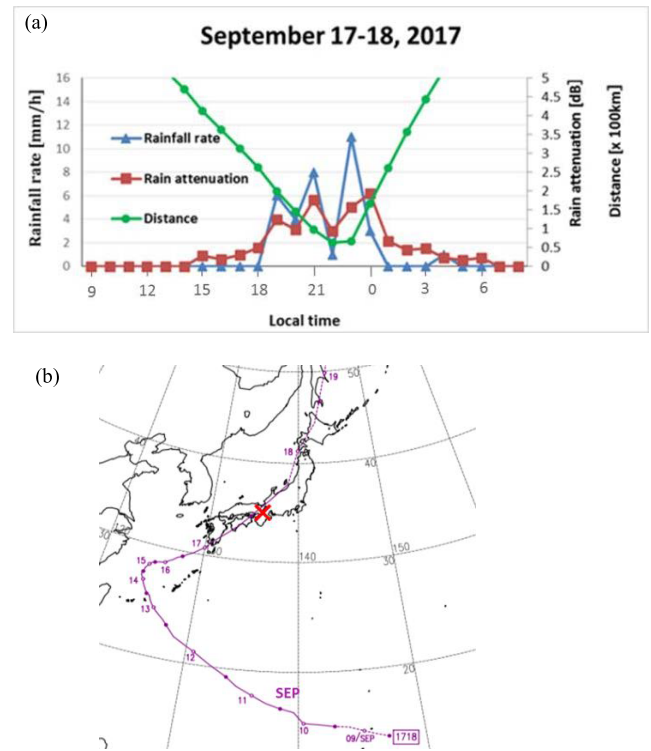


Fig. 3 (a) Rainfall rate and Ku-band rain attenuation together with typhoon distance [6] obtained on September 17–18, 2017, and (b) the typhoon route [7]. The observation point (OECU) is marked by a red cross (X).

noted that Fig. 3(a) shows the rain attenuation of as small as 2 dB, even though the typhoon approaches the station down to 50 km during 22–23 LT and the rainfall rate exceeds 10 mm/h.

Compared with the case of August 7, the degree of the attenuation due to rainfall rate is much reduced in this case. Around 23 LT on September 17, in contrast, a strong hourly southwesterly wind of 7.0 m/s was detected by the Hirakata AMeDAS [8]. Thus, the degree of attenuation due to rainfall rate is suggested to be significantly affected by the direction of ground wind velocities and the side of typhoon passage with regard to the location of the station. In this paper, velocity is used to represent a vector value composed of magnitude and direction, while speed simply means the magnitude of velocity.

3. Variation of Equivalent Path Length

In this chapter, the degree of rain attenuation due to rainfall rate is converted into equivalent path length averaged over each rainfall event. The equivalent path length L [km] is given by the rain attenuation A [dB] divided by the specific attenuation $\alpha = aR^b$ [dB/km], i.e., $L = A/\alpha$ [km], where R [mm/h] is the rainfall rate averaged over each rainfall event, and $a = 0.02308$, $b = 1.1568$ for the frequency of BS radio wave (11.84 GHz) [4]. The equivalent path lengths are calculated, using the rainfall events that lasted more than 30 min with the rainfall rates of more than 8 mm/h for sta-

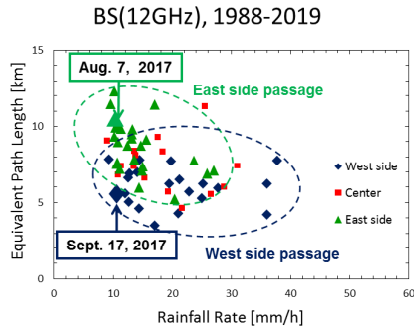


Fig. 4 Scatter gram between the average rainfall rates and equivalent path lengths for typhoon passage events obtained from 1988 to 2019. The symbols are classified by the directions of the passage.

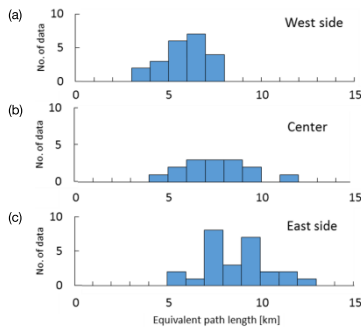


Fig. 5 Histogram of the distribution of equivalent path lengths in the case of (a) west side, (b) center, and (c) east side passage of typhoons.

tistical reliability [5].

Figure 4 shows the relationship between the average rainfall rates and equivalent path lengths for 63 typhoon passage events obtained from 1988 to 2019. These events are classified by the directions of the typhoon passage, such as west side (◆), center (■), and east side (▲), respectively. Here, the center means that the typhoon passage is near the station within the distance of about 10 km. The examples shown in Figs. 2 and 3 are indicated by the large symbols. In general, Fig. 4 indicates that the equivalent path lengths are slightly reduced as the rainfall rates are increased for each case of passage directions. Also, the equivalent path lengths tend to become longer, in the case of the east side passage (▲) than the west side passage (◆), as shown by dashed circles.

Next, the distributions of equivalent path lengths are plotted as the histogram in Fig. 5, according to the directions of the passage for (a) west side, (b) center, and (c) east side, respectively. Figure 5 shows that the equivalent path lengths are distributed from 3 to 8 km in the case of (a) the west side passage, while their distribution is increased from 5 to 13 km in the case of (c) the east side passage. The distribution for (b) the center is found between the west and east side passages.

4. Effects of Ground Wind Speed and Direction

Figure 6 shows the scatter gram between the ground wind

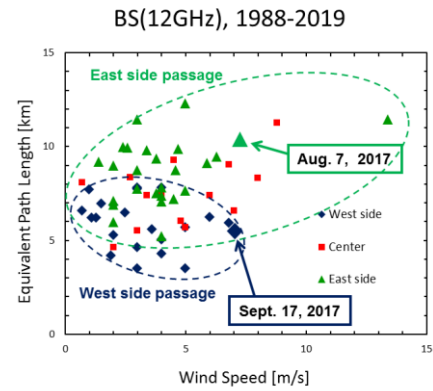


Fig. 6 Scatter gram between the ground wind speeds and the equivalent path lengths of Ku-band BS signal attenuation.

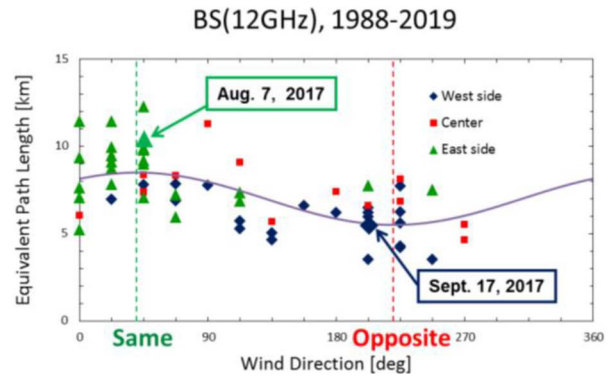


Fig. 7 Relationship between the ground wind directions and the equivalent path lengths. Dashed lines indicate wind directions along the same and opposite angles to the satellite.

speeds and the equivalent path lengths of Ku-band BS signal attenuation for the 63 typhoon passage events obtained from 1988 to 2019. Also, Fig. 7 depicts the relationship between the wind directions and the equivalent path lengths. The ground wind speed is represented by the maximal hourly value during each event. Also, the wind direction is taken from that of the maximal speed and shown clockwise from the northerly wind of 0 deg. Dashed lines in the diagram indicate wind directions along the same and opposite angles of 40.1 and 220.1 deg to the satellite, respectively. These wind speeds and directions are obtained from Hirakata AMeDAS of Japan Meteorological Agency [8], which is located 6.8 km northeast from Neyagawa station.

It is found in Fig. 6 that the equivalent path lengths of east side passage (▲) tend to be increased as the wind speeds are increased, while those of west side passage (◆) are, in contrast, rather decreased slightly. On the other hand, Fig. 7 indicates that the equivalent path lengths become larger as the wind directions approach the same angle to the satellite (40.1 deg), while they become smaller as the wind directions approach the opposite angle to the satellite (220.1 deg). Thus, the equivalent path lengths tend to become their maximum and minimum toward and against the angle to the satellite, respectively, although the data are largely scattered.

Table 2 Coefficients of specific attenuation for each satellite path.

	Frequency	Elevation	Polarization	a	b
BS	11.84 GHz	41.3 deg	Circular	0.02308	1.1568
CS	19.45 GHz	49.5 deg	Circular	0.08817	1.0253
SKP	12.6 GHz	48.8 deg	Vertical	0.02843	1.1209
SBC	12.7 GHz	48.6 deg	Vertical	0.02920	1.1184

The curve in the diagram shows the best-fit sinusoidal for the data in the least mean square sense.

Next, the relationship between the ground wind directions and the equivalent path lengths of satellite signal attenuation is similarly examined using CS (19.45 GHz), JCSAT-3 (SKP, 12.6 GHz) and SUPERBIRD-C (SBC, 12.7 GHz) other than BS (11.84 GHz). The satellite azimuth angles are 186.4 deg for CS, 193.2 deg for SKP, and 165.5 deg for SBC, respectively. The number of data in each observation period is 30 in 1988–2005 for CS, 36 in 2004–2019 for SKP, and 33 in 2004–2019 for SBC, respectively. The specification and observation period of these satellite signals used in the measurements was summarized in Table 1 in Sect. 1. Also, the observation systems and the locations of antennas used in the measurements were shown in Fig. 1. In addition, the coefficients a and b of the specific attenuation $\alpha = aR^b$ are summarized here in Table 2 for frequency, elevation angle, and polarization of each satellite [4].

Figure 8 depicts the relationships between the ground wind directions and the equivalent path lengths of the satellite signal attenuation for (a) CS, (b) SKP, and (c) SBC, respectively. Figure 8 also indicates that the equivalent path lengths become larger as the wind directions approach the same angle to each satellite, while they become smaller as the wind directions approach the opposite angle to each satellite, as shown by the best-fit sinusoidal curves, respectively.

5. Relationship between Ground Wind Velocity and Equivalent Path Lengths

In the previous chapter, the ground wind velocities obtained by the nearby AMeDAS station in the typhoon events are clearly shown to affect the equivalent path length of rain attenuation on various satellite propagation paths, such as BS, CS, SKP, and SBC. Especially, the wind direction as well as the wind speed is found to be essential to increase and decrease of the equivalent path lengths according to the various azimuth angles of these satellites. In this chapter, a simple propagation path model to explain possible effects of wind velocity to the observed equivalent path length is considered, based on the relationship between horizontal wind speed along the propagation path and fall velocities of raindrops.

Figure 9 shows the model of the slant path length for the rain height H (km), the satellite elevation angle ϕ (deg), and the homogeneous rain area with average rainfall rate R (mm/h). The rain height is here represented by 0°C isotherm height. In the case of Fig. 9(a) without the effects of horizontal wind speed along the propagation path,

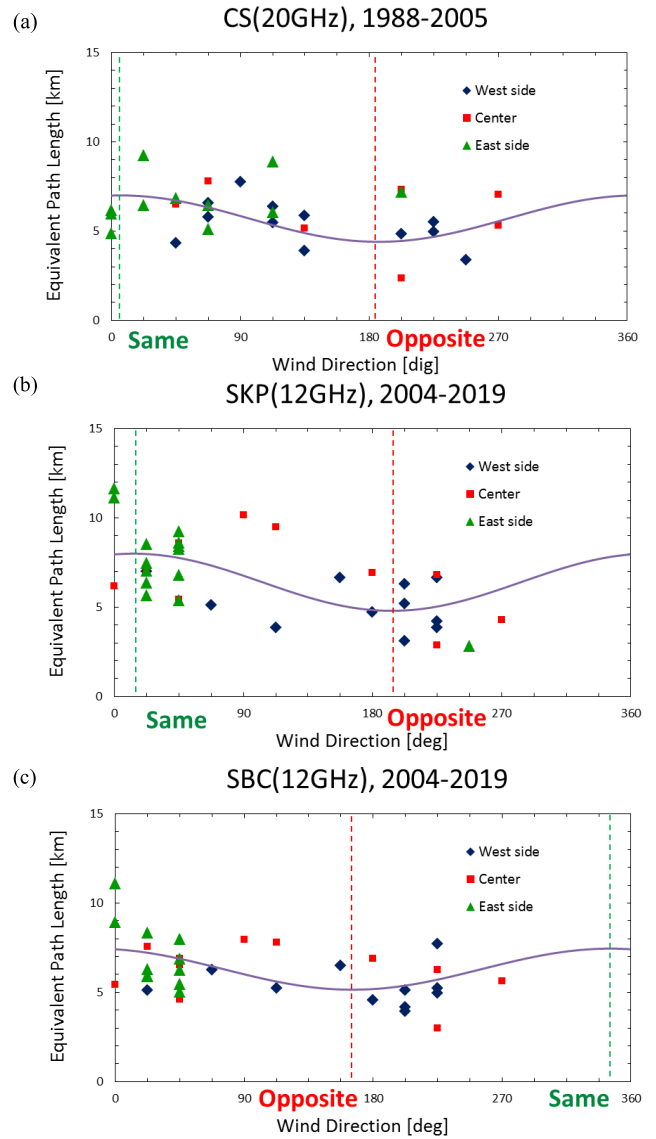


Fig. 8 Relationship between the ground wind directions and the equivalent path lengths of the satellite signal attenuation for (a) CS, (b) SKP, and (c) SBC, respectively. Dashed lines indicate wind directions along the same and opposite angles to each satellite.

the raindrops fall down vertically and pass through the rain area with rainfall rate R (mm/h) straightly.

In the case of Fig. 9(b) with the horizontal wind speed toward the same angle to the satellite, however, the horizontal advection is added to the fall velocities of raindrops, and the fall direction moves toward the direction to the satellite. This means substantial increase in the rain area with rainfall rate R (mm/h) across the propagation path as shown by the dark shaded area. On the other hand, when the horizontal wind speed is opposite to the direction to the satellite as shown in Fig. 9(c), the fall direction of raindrops moves against the direction to the satellite, and this causes the substantial decrease in the rain area with rainfall rate R (mm/h) as shown by the thin shaded area.

To estimate more quantitatively these substantial in-

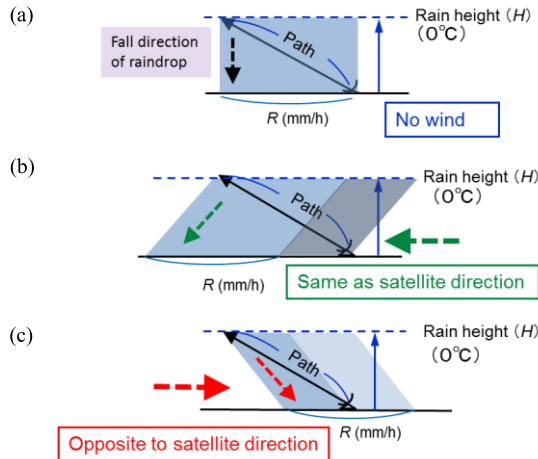


Fig. 9 Model of the slant path length for the rain height H (km), the satellite elevation angle ϕ (deg), and average rainfall rate R (mm/h), in the case of (a) no wind, (b) the horizontal wind direction same as the angle to the satellite, and (c) opposite to the angle to the satellite.

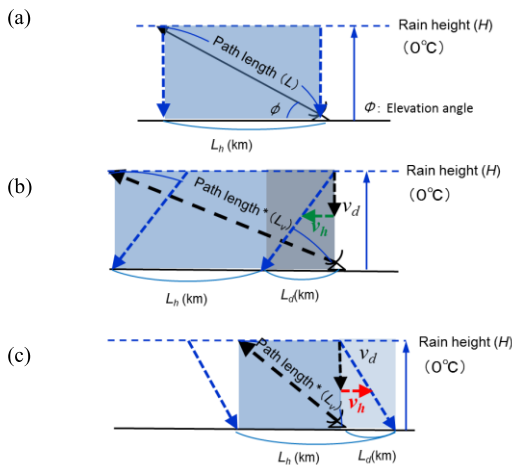


Fig. 10 Slant path lengths modified by including the horizontal advection of raindrops in the case of (a) no wind, (b) the horizontal wind direction same as the angle to the satellite, and (c) opposite to the angle to the satellite. The fall direction of raindrops is considered to be apparently vertical.

crease and decrease in the rain area across the propagation path due to the horizontal wind speed, the slant path lengths in the rain area of Fig. 9 are modified so that the fall direction of raindrops becomes apparently vertical in Fig. 10. The slant path lengths are then modified including the horizontal advection of raindrops.

As shown in Fig. 10(a), the original slant-path length L below the rain height H is given by

$$L = H / \sin \phi \quad (\text{km}) \quad (1)$$

where ϕ is the satellite elevation angle, and the height of the earth station is assumed to be 0 km, so reduction of the rain height is here omitted. In Fig. 10(a) without the effects of horizontal wind speed, the horizontal projection L_h of the rain height is simply given by

$$L_h = L \cos \phi = H \cot \phi \quad (\text{km}) \quad (2)$$

In Fig. 10(b) with the horizontal wind speed toward the angle to the satellite, however, the increase of the horizontal projection L_d due to the advection of raindrops is expressed by

$$L_d = H \left(\frac{v_h}{v_d} \right) \quad (\text{km}) \quad (3)$$

where v_h (m/s) is the horizontal wind speed, and v_d (m/s) is the vertical fall speed of raindrops. The horizontal advection of raindrops is here assumed to be the same as the horizontal wind speed v_h , which is also considered to be nearly constant from the ground to the rain height for typhoon events with a large vortex of the atmospheric motion. The agreement between the ground wind velocity and the upper air flow is discussed in the next chapter. On the other hand, the vertical fall speed of raindrops is, in general, known to distribute from 1 to 9 m/s, according to the diameter of raindrops from 0.2 to 5.8 mm by the earlier measurements in stagnant air [9]. In this calculation, the average fall speed is assumed to be 6 m/s in light of the recent observations by wind profilers [10].

In the case of Fig. 10(c) with the horizontal wind speed against the angle to the satellite, L_d means the decrease of the horizontal projection with the minus value, which is similarly expressed by the minus values of v_h . Thus, with the apparent vertical fall direction of raindrops, the correction of the slant-path length* L_v , hereinafter referred to as modified equivalent path length, including the effects of the horizontal advection of raindrops v_h is readily given by

$$L_v = \sqrt{(L_h + L_d)^2 + H^2} = H \times \sqrt{\left(\cot \phi + \left(\frac{v_h}{v_d} \right) \right)^2 + 1} \quad (4)$$

Next, Fig. 11 shows the relationship between the horizontal ground wind speeds along the satellite propagation paths and the equivalent path lengths observed by (a) BS with azimuth angle of 220.1 deg, (b) CS with 186.4 deg, (c) SKP with 193.2 deg, and (d) SBC with 165.5 deg, respectively. In these diagrams, the horizontal wind speeds are projected to the radio wave propagation direction along the angle to each satellite, where the positive speed means wind direction toward the angle to the satellite, and the negative speed means wind direction opposite to the angle to the satellite, respectively.

For each propagation path, the equivalent path lengths are found to indicate a good correlation with the ground wind speeds along the angle to each satellite. In the case of the west side passage (◆), the wind speeds tend to become opposite to the direction to each satellite with minus values, yielding shorter equivalent path lengths of less than 5 km. In the case of the east side passage (▲), in contrast, the wind speeds tend to become positive values, giving rise to longer equivalent path length up to 10 km for all the satellite paths.

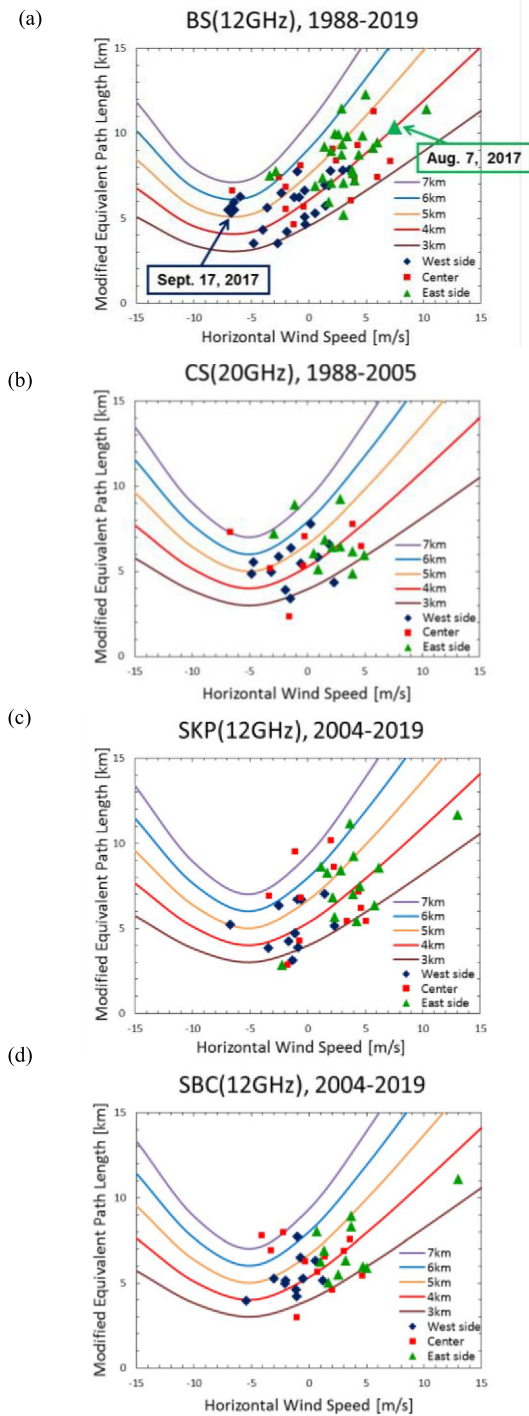


Fig. 11 Relationship between the horizontal ground wind speeds along the satellite propagation paths and the equivalent path lengths observed by (a) BS, (b) CS, (c) SKP, and (d) SBC, respectively. Solid lines indicate the modified equivalent path length calculated from Eq. (4) for each horizontal wind speed with the rain height of 3–7 km.

Solid lines in the diagrams indicate the modified equivalent path length L_v calculated from Eq. (4) for each horizontal speed v_h with the rain height H of 3–7 km. The vertical fall speed of raindrops v_d is assumed to be 6 m/s, as was mentioned before. The satellite elevation angles ϕ are (a)

41.3 deg for BS, (b) 49.5 deg for CS, (c) 48.8 deg for SKP, and (d) 48.6 deg for SBC, respectively, as was listed in Table 1 in Sect. 1.

These calculated curves of the modified equivalent path length for each satellite show a good agreement with the observed equivalent path lengths, strongly suggesting the effects of horizontal wind speed to the increase and decrease of path length. Also, the equivalent path lengths of each satellite tend to become the minimum of the rain height itself, for both modified and observed values at the wind speed around -5 to -6 m/s. At this speed, the fall direction of raindrops shown by the thin red broken arrow in Fig. 9(c) coincides with the satellite elevation angle, so the equivalent path length is considered to be the minimum because $\frac{v_h}{v_d} = -\cot \phi$ and $L_v = H$ in Eq. (4).

6. Effects of the Upper Air Flow

The radio wave propagation paths should be affected by the upper air flow as well as the ground wind speed, as was mentioned in the preceding chapter. Fortunately in our previous studies [11], [12], the rain area motions causing rain attenuation were estimated by two kinds of BS signal three-point observations. One of the three points in the wide area of 20–50 km consists of Osaka Electro-Communication University (OECU, Neyagawa, Osaka), Kyoto University (RISH, Uji, Kyoto), and Shigaraki MU radar (MU, Koga, Shiga). The other of the three points in the narrow area of 3–8 km consists of Osaka Electro-Commun. Univ. (OECU, Neyagawa) and two other premises of our university at Moriguchi and Shijonawate cities. The locations of these three-point BS signal observations in the wide and narrow areas are illustrated in Fig. 12.

The rain area motions inferred from the time difference of cross-correlation functions among the three-point BS signal observations were found to agree well with the motions of rain fronts or low atmospheric pressure, such as extratropical cyclones [11]. Also, the rain area motions were shown to correspond to the upper air flow around the rain height of 4 km detected by the simultaneous MU radar wind observations [13].

Figure 13 shows (a) the wind velocities observed on the ground by the Hirakata AMeDAS and (b) the upper air flows inferred from rain area motions by the three-point BS signal observations in the typhoon events from 2004 to 2013. The ground wind velocities are based on the average of one-hour AMeDAS data, while the rain area motions are obtained from the time difference of cross-correlation functions among the three-point BS signal observations from one to a few hours. In addition, Fig. 14 depicts the scatter grams of (a) wind speeds and (b) wind directions between the ground wind velocities of AMeDAS and the rain area motions of the three-point observations shown in Fig. 13, respectively.

In Fig. 13, the plus velocities indicate eastward and northward directions, while the minus velocities indicate westward and southward directions. In Fig. 14(b), on the

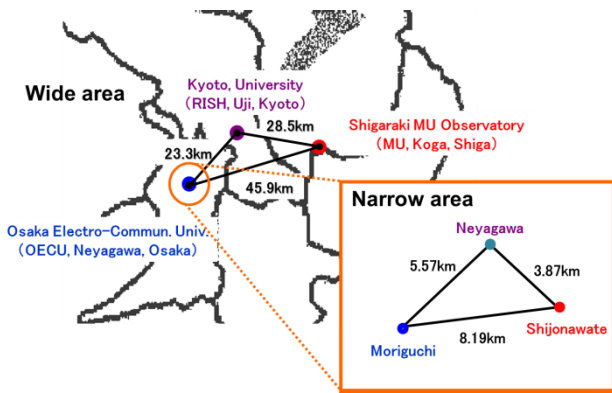


Fig. 12 Locations of wide and narrow area three-point observations of the BS signals.

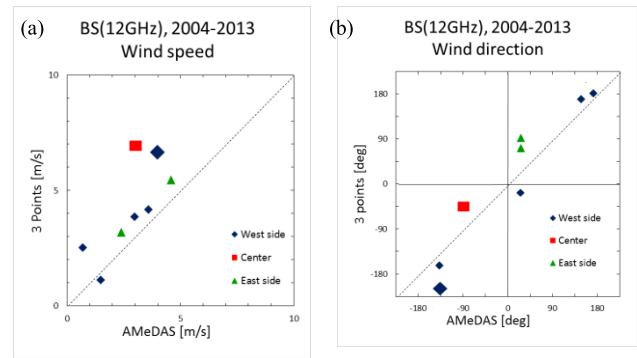


Fig. 14 Scatter grams of (a) wind speeds and (b) wind directions between the ground wind velocities observed by AMeDAS and the upper air flow inferred by the three-point BS signal observations.

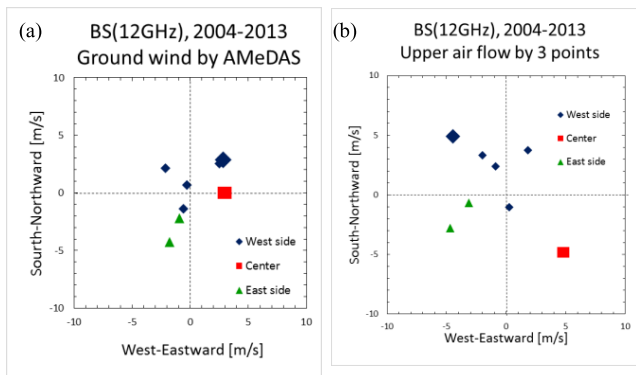


Fig. 13 (a) Ground wind velocities observed by AMeDAS and (b) upper air flow inferred from rain area motions by the three-point BS signal observations in the typhoon events from 2004 to 2013.

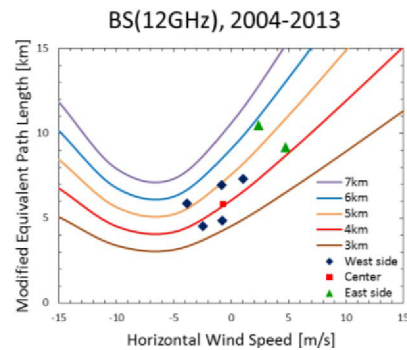


Fig. 15 Relationship between the horizontal wind speeds in the air along the satellite propagation paths and the equivalent path lengths observed by BS in 2004–2013. Solid lines indicate the modified equivalent path length calculated from Eq. (4).

other hand, the 0 deg is the northerly wind direction, and the plus and minus angles mean clockwise and ant-clockwise rotations, respectively. In Figs. 13 and 14, the two large symbols indicate the data points obtained by the three-point observations in the wide area in 2004, while the others are those obtained by the three-point observations in the narrow area after 2005.

Figs. 13 and 14 indicate that the ground wind velocities agree fairly well with the upper air flows in both wind speeds and directions in spite of the difference of about 4 km between the ground and rain heights. Note that two points of wind speed data with large symbols in Fig. 14(a) have slightly larger values exceeding 6 m/s, for the three-point observation in the wide area of 20–50 km. The three-point observations obtained from the narrow area of 3–8 km, however, indicate a better correspondence to the ground wind speeds, possibly due to a more localized observation area.

In the case of the rain events other than typhoon such as cold or stationary rain fronts, in contrast, the ground wind velocities by AMeDAS usually indicated by nearly one order smaller values, compared with the upper-air rain area motions inferred by the three-point BS signal observations [14]. In the present typhoon events, however, the ground wind velocities coincide well with the rain area motions, as

shown in Figs. 13 and 14. Therefore, the calculations of the equivalent path lengths, demonstrated in Fig. 11 in the preceding chapter, seem to well represent the effects of upper air flow from the ground to the rain height. The correspondence between ground wind velocity and upper air flow was also confirmed by the observations with the MU and boundary layer radar in a typhoon event. The ground wind speeds and directions almost the same as those of the westward upper air flow were demonstrated during the typhoon passage in the east side of the MU radar [15].

Finally, Fig. 15 shows the relationship between the horizontal wind speeds in the air along the satellite propagation paths and the equivalent path lengths observed by BS in 2004–2013. The horizontal wind velocities are here averaged by vector mean values between the ground velocities and the upper air flows shown in Fig. 13(a) and (b), respectively. Solid lines similarly indicate the modified equivalent path length calculated from Eq. (4). These calculated curves of the modified equivalent path length also show a good agreement with the observed equivalent path lengths, suggesting the effects of upper-air horizontal wind speed to the path length. Thus, the horizontal wind velocities obtained from the vector mean values averaged between the ground and rain height well represent the upper air flow along the

propagation path.

7. Conclusions

The rain attenuation characteristics due to typhoon passage are discussed using Ku-band BS satellite signal observations conducted in Neyagawa, Osaka, from 1988 to 2019. The 63 rainfall events are examined when the typhoon approaches the station. The degree of hourly rain attenuation due to rainfall rate is found to be largely enhanced as the typhoon passes the east side of the station. The equivalent path lengths averaged over each rainfall event become 5–13 km in the case of east side typhoon passage, while they stay 3–8 km in the case of west side passage.

Compared with the hourly ground wind velocities obtained from nearby AMeDAS, the equivalent path lengths of east side passage are shown to be increased as the wind speeds are increased, although those of west side passage are decreased slightly. It is also found that the equivalent path lengths become larger as the wind directions approach the same angle to the satellite, while they become smaller as the wind directions approach the opposite angle to the satellite. Furthermore, these increase and decrease of the equivalent path lengths are confirmed in other Ku-band and Ka-band satellite paths with different azimuth angles, such as CS, SKP, and SBC.

The modified equivalent path lengths calculated by a simple propagation path model, including the effects of horizontal wind speeds to fall velocities of raindrops, agree well with the equivalent path length observed by each satellite. Also, in the typhoon events the upper air flows are shown to be almost the same as the ground wind velocities by the three-point BS signal observations. The effects of the upper air flow to the equivalent path lengths are confirmed at the same time. Thus, this study has, for the first time, proved that the equivalent path lengths of the rain attenuation should be largely affected by the direction of typhoon passage and the horizontal wind velocities. Further study is needed for the effects of wind velocities to the equivalent path length in rainfall events other than typhoon events, such as extratropical cyclones or low atmospheric pressure events with warm, cold, and stationary rain fronts.

Acknowledgments

The authors deeply thank Mrs. S. Sasaki, K. Yamasaki, and S. Nishimura who graduated from Osaka Electro-Communication University for assisting the data analyses.

References

- [1] H. Fukuchi, T. Kozu, K. Nakamura, J. Awaka, H. Inomata, and Y. Otsu, "Centimeter wave propagation experiments using the beacon signals of CS and BSE satellite," *IEEE Trans. Antennas Propag.*, vol.AP-31, no.4, pp.603–613, July 1983.
- [2] Y. Karasawa and Y. Maekawa, "Ka-band earth-space propagation research in Japan," *Proc. IEEE*, vol.85, no.6, pp.821–841, June 1997.
- [3] S. Nakazawa, S. Tanaka, and K. Shogen, "A method to transform

rainfall rate to rain attenuation and its application to 21 GHz band satellite," *IEICE Trans. Commun.*, vol.E91-B, no.6, pp.1806–1811, June 2008.

- [4] "Propagation data and prediction methods required for the design of earth-space telecommunication systems," Geneva, ITU-R Recommendation, p.618-13, 2017.
- [5] Y. Maekawa, "A study on long-term rain attenuation characteristics in Ka and Ku band satellite communications," *Proc. 29th AIAA International Communications Satellite Systems Conference (ICSSC-2011)*, ICSSC-17-1, Nara, Nov.-Dec. 2011.
- [6] <http://agora.ex.nii.ac.jp/digital-typhoon/year/>
- [7] https://www.data.jma.go.jp/yoho/typhoon/route_map/index.html
- [8] <https://www.data.jma.go.jp/obd/stats/etm/index.php>
- [9] R. Gunn and G.D. Kinzer, "The terminal velocity of fall for water droplets in stagnant air," *J. Meteor.*, vol.6, no.4, pp.243–248, 1949.
- [10] C.R. Williams and W.L. Wcklund, "Classification of precipitation clouds in the tropics using 915-MHz wind profilers," *J. Atmos. Oceanic. Technol.*, vol.12, no.5, pp.996–1012, 1995.
- [11] Y. Maekawa, T. Nakatani, Y. Shibagaki, and T. Hatsuda, "A study on site diversity techniques related to rain area motion using Ku-band satellite signals," *IEICE Trans. Commun.*, vol.E91-B, no.6, pp.1812–1818, June 2008.
- [12] Y. Maekawa, K. Sawai, Y. Shibagaki, T. Takami, and K. Hatsuda, "Site diversity effects on Ku-band satellite signal attenuation related to rain area motion," *Proc. ISAP2008*, 3A07-3, Taipei, Taiwan, Oct. 2008.
- [13] M. Noyama, Y. Shibagaki, and Y. Maekawa, "Rain attenuation characteristics of Ku-band satellite signals related to radar observations of the wind velocities at rain height," *Proc. 29th AIAA International Communications Satellite Systems Conference (ICSSC-2011)*, ICSSC-17-2, Nara, Nov.-Dec. 2011.
- [14] Y. Inamori, Y. Shibagaki, and Y. Maekawa, "Rain attenuation characteristics of Ku-band satellite signals in relation to the wind velocities observed on the ground," *Proc. ISAP 2012*, 4D3-4, P0235, Nagoya, Japan, Oct.–Nov. 2012.
- [15] M. Teshiba, H. Hashiguchi, S. Fukao, and Y. Shibagaki, "Typhoon 9707 observations with MU radar and L-band boundary layer radar," *Ann. Geophys.*, vol.19, no.8, pp.925–931, 2001.



Yasuyuki Maekawa received the B.S., M.S., and Ph.D. degrees in electronics engineering from Kyoto University in 1979, 1981, and 1985, respectively. In 1985, he joined the Department of Tele-communication Engineering, Osaka Electro-Communication University, Neyagawa, Osaka, Japan, where he is currently a Professor of satellite communication engineering. His research activities are concerned with microwave and millimeter wave propagation on the earth-space paths and meteorological radar

observations of the atmosphere. Dr. Maekawa is a Member of Institute of Electrical and Electronics Engineers (IEEE), the Society of Geomagnetism and Earth, Planetary and Space Science, and the Meteorological Society of Japan.



Yoshiaki Shibagaki received the B.S., M.S., and Ph.D. degrees in communication engineering from Osaka Electro-Communication University in 1992, 1994, and 1997, respectively. After working as a research fellow PD of the Japan Society for the Promotion of Science (JSPS) in Kyoto University, Uji, Kyoto, he joined Department of Telecommunication Engineering, Osaka Electro-Communication University in 1999. He is currently a Professor of applied radio wave engineering including re-

mote sensing techniques. His main research activities are observations of mesoscale meteorology using atmospheric and meteorological radars. He is a Member of the Meteorological Society of Japan.